Journal of
Neurology, Neurosurgery
& Psychiatry

Attack-related damage of Thalamic Nuclei in Neuromyelitis Optica Spectrum Disorders

Journal:	*Journal of Neurology, Neurosurgery, and Psychiatry*
Manuscript ID	jnnp-2018-320249.R1
Article Type:	Research paper
Date Submitted by the Author:	n/a
Complete List of Authors:	Papadopoulou, Athina; NeuroCure Clinical Research Center, Charité – Universitätsmedizin Berlin, corporate member of Freie Universität Berlin, Humboldt-Universität zu Berlin, and Berlin Institute of Health; University Hospital of Basel , Neurology Oertel, Frederike; NeuroCure Clinical Research Center, Charité – Universitätsmedizin Berlin, corporate member of Freie Universität Berlin, Humboldt-Universität zu Berlin, and Berlin Institute of Health Gaetano, Laura; Medical Image Analysis Center ; University Hospital of Basel , Neurology Kuchling, Joseph; NeuroCure Clinical Research Center, Charité – Universitätsmedizin Berlin, corporate member of Freie Universität Berlin, Humboldt-Universität zu Berlin, and Berlin Institute of Health Zimmermann, Hanna; NeuroCure Clinical Research Center, Charité – Universitätsmedizin Berlin, corporate member of Freie Universität Berlin, Humboldt-Universität zu Berlin, and Berlin Institute of Health Chien, Claudia; NeuroCure Clinical Research Center, Charité – Universitätsmedizin Berlin, corporate member of Freie Universität Berlin, Humboldt-Universität zu Berlin, and Berlin Institute of Health Siebert, Nadja; NeuroCure Clinical Research Center, Charité – Universitätsmedizin Berlin, corporate member of Freie Universität Berlin, Humboldt-Universität zu Berlin, and Berlin Institute of Health Asseyer, Susanna; NeuroCure Clinical Research Center, Charité – Universitätsmedizin Berlin, corporate member of Freie Universität Berlin, Humboldt-Universität zu Berlin, and Berlin Institute of Health Bellmann-Strobl, Judith; NeuroCure Clinical Research Center, Charité – Universitätsmedizin Berlin, corporate member of Freie Universität Berlin, Humboldt-Universität zu Berlin, and Berlin Institute of Health; Experimental and Clinical Research Center, Max Delbrueck Center for Molecular Medicine and Charité – Universitätsmedizin Berlin, corporate member of Freie Universität Berlin, Humboldt-Universität zu Berlin, and Berlin Institute of Health Ruprecht, Klemens; Charité – Universitätsmedizin Berlin, corporate member of Freie Universität Berlin, Humboldt-Universität zu Berlin, and Berlin Institute of Health, Department of Neurology; NeuroCure Clinical Research Center, Charité – Universitätsmedizin Berlin, corporate member of Freie Universität Berlin, Humboldt-Universität zu Berlin, and Berlin Institute of Health Chakravarty, Mallar; Cerebral Imaging Centre, Douglas Mental Health University Institute; McGill University Department of Psychiatry and

	Department of Biomedical Engineering Scheel, Michael; Charité – Universitätsmedizin Berlin, corporate member of Freie Universität Berlin, Humboldt-Universität zu Berlin, and Berlin Institute of Health, Department of Neuroradiology; NeuroCure Clinical Research Center, Charité – Universitätsmedizin Berlin, corporate member of Freie Universität Berlin, Humboldt-Universität zu Berlin, and Berlin Institute of Health Magon, Stefano; University Hospital Basel, Neurology; Medical Image Analysis Center Wuerfel, Jens; Medical Image Analysis Center Paul, Friedemann; NeuroCure Clinical Research Center, Charité – Universitätsmedizin Berlin, corporate member of Freie Universität Berlin, Humboldt-Universität zu Berlin, and Berlin Institute of Health; Experimental and Clinical Research Center, Max Delbrueck Center for Molecular Medicine and Charité – Universitätsmedizin Berlin, corporate member of Freie Universität Berlin, Humboldt-Universität zu Berlin, and Berlin Institute of Health Brandt, Alexander; NeuroCure Clinical Research Center, Charité – Universitätsmedizin Berlin, corporate member of Freie Universität Berlin, Humboldt-Universität zu Berlin, and Berlin Institute of Health; Department of Neurology, University of California Irvine
Keywords:	
Specialty:	

Attack-related damage of Thalamic Nuclei in Neuromyelitis Optica Spectrum Disorders

Athina Papadopoulou, MD[1-3], Frederike C. Oertel[1], Laura Gaetano, PhD[2,4,5], Joseph Kuchling, MD[1], Hanna G. Zimmermann, PhD[1], Claudia Chien, MSc[1], Nadja Siebert, MD[1], Susanna E. Asseyer[1], Judith Bellmann-Strobl, MD[1,3], Klemens Ruprecht, MD[1,6], M. Mallar Chakravarty, PhD[7-8], Michael Scheel, MD[1,9], Stefano Magon, PhD[2,4], Jens Wuerfel, MD[4], Friedemann Paul, MD[1,3,6], Alexander U. Brandt, MD[1,10]

AUTHORS AFFILIATIONS:

1) NeuroCure Clinical Research Center, Charité – Universitätsmedizin Berlin, corporate member of Freie Universität Berlin, Humboldt-Universität zu Berlin, and Berlin Institute of Health, Berlin, Germany

2) Department of Neurology, University and University Hospital Basel, Switzerland

3) Experimental and Clinical Research Center, Max Delbrueck Center for Molecular Medicine and Charité – Universitätsmedizin Berlin, corporate member of Freie Universität Berlin, Humboldt-Universität zu Berlin, and Berlin Institute of Health, Berlin, Germany

4) Medical Image Analysis Center (MIAC AG) and Department for Biomedical Engineering Basel, Switzerland

5) F. Hoffmann–La Roche, Basel, Switzerland

6) Department of Neurology, Charité – Universitätsmedizin Berlin, corporate member of Freie Universität Berlin, Humboldt-Universität zu Berlin, and Berlin Institute of Health, Berlin, Germany

7) Cerebral Imaging Centre, Douglas Mental Health University Institute, Montreal, Canada

8) McGill University Department of Psychiatry and Department of Biomedical Engineering, Montreal, Canada

9) Department of Neuroradiology, Charité – Universitätsmedizin Berlin, corporate member of Freie Universität Berlin, Humboldt-Universität zu Berlin, and Berlin Institute of Health, Berlin, Germany

10) Department of Neurology, University of California Irvine, CA, USA

CORRESPONDING AUTHOR

Alexander U. Brandt

NeuroCure Clinical Research Center

Charité – Universitätsmedizin Berlin

Charitéplatz 1, DE-10117, Berlin, Germany

Telephone: +49-30-450-539797

Fax: +49-30-450-539915

Email: alexander.brandt@charite.de

ORCID ID: 0000-0002-9768-014X

KEYWORDS: thalamus, neurodegeneration, optic neuritis, anterograde degeneration

PAPER INFORMATION:

Character count of full title: 80

Word count of the entire manuscript: 3500

Word count of the Abstract: 250

Number of tables and figures: 8 (4 tables and 4 figures)

References: 40

Supplementary material

LIST OF ABBREVIATIONS:

AQP4= aquaporin-4, cR^2= conditional R^2, EDSS= expanded disability status scale, GCIPL= ganglion cell-inner plexiform layer, LETM= longitudinal extensive transverse myelitis, LGN=lateral geniculate nucleus, logMAR= logarithm of the minimum angle of resolution, mR^2= marginal R^2, MAGeT= Multiple Automatically Generated Templates, MRI= magnetic resonance imaging, NMO-NON: patients with NMOSD and no prior optic neuritis, NMO-ON: patients with NMOSD and prior optic neuritis, NMOSD= neuromyelitis optica spectrum disorders, ON= optic neuritis, OR= optic radiations, pRNFL= peripapillary retinal nerve fiber layer, SE= standard error, VPN= ventral posterior nucleus

ABSTRACT

OBJECTIVES: In neuromyelitis optica spectrum disorders (NMOSD) thalamic damage is controversial, but thalamic nuclei were never studied separately. We aimed at assessing volume loss of thalamic nuclei in NMOSD. We hypothesized that only specific nuclei are damaged, by attacks affecting structures from which they receive afferences: the lateral geniculate nucleus (LGN), due to optic neuritis (ON) and the ventral posterior nucleus (VPN), due to myelitis.

METHODS: Thirty-nine patients with aquaporin 4-IgG seropositive NMOSD (age:50.1±14.1 years, 36 women, 25 with prior ON, 36 with prior myelitis) and 37 healthy controls (age:47.8±12 years, 32 women) were included in this cross-sectional study. Thalamic nuclei were assessed in magnetic resonance images, using a multi-atlas-based approach of automated segmentation. Retinal optical coherence tomography was also performed.

RESULTS: Patients with ON showed smaller LGN volumes (181.6±44.2 mm^3) compared to controls (198.3±49.4 mm^3; B=-16.97, p=0.004) and to patients without ON (206.1±50 mm^3; B=-23.74, p=0.001). LGN volume was associated with number of ON episodes (Rho=-0.536, p<0.001), peripapillary retinal nerve fiber layer thickness (B=0.70, p<0.001) and visual function (B=-0.01, p<0.001). Although VPN was not smaller in patients with myelitis (674.3±67.5 mm^3) than controls (679.7±68.33; B=-7.36, p=0.594), we found reduced volumes in five patients with combined myelitis and brainstem attacks (B=-76.18, p=0.017). Volumes of entire thalamus and other nuclei were not smaller in patients than controls.

CONCLUSION: These findings suggest attack-related anterograde degeneration rather than diffuse thalamic damage in NMOSD. They also support a potential role of LGN volume as an imaging marker of structural brain damage in these patients.

INTRODUCTION

Neuromyelitis optica spectrum disorders (NMOSD) are chronic, relapsing inflammatory disorders of the central nervous system, defined by pathogenic IgG antibodies against astrocytic aquaporin-4 (AQP4-IgG) in the majority of cases[1]. The most typical clinical manifestations are optic neuritis (ON) and acute myelitis, usually occurring as longitudinally extensive transverse myelitis[1,2]. Other clinical core characteristics include area postrema and acute brainstem syndromes[1].

Patients with NMOSD very rarely show a secondary progressive phase[3], and the mechanisms leading to neurological disability are thought to be mainly attack-related[3–5]. However, recent findings suggested retinal neuronal loss independent of ON attacks in NMOSD[6]. Moreover, some imaging[7,8] and histopathological studies in NMOSD[9,10] showed abnormalities and neuronal loss in non-lesional cortical grey matter. Less is known regarding deep grey matter changes in NMOSD, particularly the affection of the thalamus is controversial[11–16].

Our aim was to assess volume loss in thalamic nuclei in NMOSD. Our hypothesis was that lesions in i) the optic nerve due to ON and ii) the spinal cord due to myelitis may cause anterograde degeneration only to specific nuclei, with which these structures are connected. We hypothesized that the lateral geniculate nucleus (LGN), which receives afferences from the optic nerve, is affected due to ON and the ventral posterior nucleus (VPN), which receives afferences from the dorsal column-medial lemniscal pathway and the spinothalamic tract, due to myelitis (Fig. 1). Thus, we assessed LGN and VPN

volumes in NMOSD, and studied whether they are associated to clinical attacks (ON, myelitis), attack-related structural damage (in retina and spinal cord) and clinical deficits (visual and sensory dysfunction). Our secondary, exploratory objective was to investigate whether there is occult volume loss in other thalamic nuclei in NMOSD.

METHODS

Study participants

We screened 78 patients with NMOSD from a prospective observational cohort study at the NeuroCure Clinical Research Center at the Charité-Universitätsmedizin Berlin (recruited from May 2013 to January 2018). The inclusion criteria were: i) age ≥18 years and ii) AQP4-IgG seropositive NMOSD, according to the 2015 International Consensus Diagnostic Criteria[1]. AQP4-IgG were determined by a cell-based assay (Euroimmun, Lübeck, Germany). Patients that were AQP4-IgG seronegative (n=25), had incomplete clinical data and/or unknown AQP4-IgG-status (n=10), no MRI data (n=3) or an attack within three months prior to baseline (n=1) were excluded.

We included 39 AQP4-IgG seropositive NMOSD patients. Data from 37 healthy controls with age ≥18 years, without history of neurological or opthalmological diseases were also included. Helathy controls were chosen from the institute's research database, to be as well matched as possible regarding age and sex to the patients. The characteristics of the study participants are presented in table 1.

Table 1: Characteristics of the NMOSD patients and controls included in the study

	NMOSD Patients (n=39)	Controls (n=37)

Aquaporin 4 IgG antibodies (seropositive, %)	39 (100%)	-
Age, years (mean ± SD)	50.1 ± 14.1	47.8 ± 12.5
Sex, female/male (female %)	36/3 (92.3%)	32/5 (86.5%)
Handedness (right/left)	34/4	33/2
Race (White/Black/Asian)	37/1/1	37/0/0
Disease duration, years (mean ± SD)	8.8 ± 8	-
Total number of previous attacks (median, range)	3 (1-22)	-
Patients with ON (n, %)	25 (64.1%)	-
Number of ON episodes per patient (median, range)	1 (0-12)	-
Time since fist ON episode, years (mean ± SD)	9.6 ± 7.5	-
Time since last ON episode, years (mean ± SD)	5.4 ± 3.7	-
Visual acuity, logMAR (mean ± SD)	0.24 ± 0.71	-0.01 ± 0.22
pRNFL thickness, μm (mean ± SD)	79.1 ± 21.2	96.0 ± 9.2
GCIPL volume, mm^3 (mean ± SD)	1.6 ± 0.3	1.9 ± 0.2
Patients with myelitis (n, %)	36 (92.3%)	-

Number of myelitis episodes per patient (median, range)	1 (0-15)	-
Time since fist myelitis episode, years (mean ± SD)	7.4 ± 6.7	-
Time since last myelitis episode, years (mean ± SD)	4.3 ± 3.4	-
Patients with LETM in MRI at study baseline (n, %)	22 (56.4%)	-
Sensory Functional System Score (median, range)	2 (0-4)	-
Patients with brainstem attacks (n, %)	5 (12.8%)	-
EDSS (median, range)	4 (0-7)	-
Patients with other autoimmune diseases (n, %)	13 (33.3%)	-
Patients on immunosuppressive treatment at study baseline (n, %)	34 (87.2%)	-
Patients on daily corticosteroids at study baseline (n, %).	7 (17.9%)	-

Note that there were 25 patients with previous ON; from them, 22 had both ON- and myelitis history, while 3 had only ON history, without myelitis.

Visual acuity was tested monoocularly and thus the mean logMAR refers to the mean of both eyes.

The presence of LETM (defined as spinal cord lesions extending over at least 3 vertebrae) was evaluated at study baseline, i.e. months or years after the myelitis episodes.

Note that from the five patients that were not on immunosuppressive treatment at study baseline, only two were permanently untreated, due to severe leucopenia and long-term prednisone therapy, respectively. The other three were untreated at this time-point, due to side effects of previous treatments, but received immunosuppression later. Note also that seven patients were receiving daily oral steroids (prednisolone) at study baseline: one at a dose of 2mg/day, five at 5mg/day and one at 50mg/day.

Abbreviations: EDSS= Expanded Disability Status Scale, LETM= longitudinal extensive transverse myelitis, logMAR= Logarithm of the Minimum Angle of Resolution, MRI= magnetic resonance imaging, NMOSD= neuromyelitis optica spectrum disorders, ON= optic neuritis, SD= standard deviation.

This study was approved by the local ethics committee (Ethikkommission der Charité – Universitätsmedizin Berlin; EA1/131/09) and conducted in accordance with the declaration of Helsinki in its currently applicable version. All participants gave written informed consent before inclusion in the study.

Clinical assessment

Comprehensive neurological examinations were performed by raters, under supervision of board certified neurologists, to assess the Expanded Disability Status Scale (EDSS), including the functional system scores (FSS) according to the Neurostatus definitions. Attack history was also recorded, using clinical criteria.

Visual acuity was tested monocularly under photopic conditions using retroilluminated Early Treatment in Diabetes Retinopathy Study charts at a four-meter distance. The

logarithm of the minimum angle of resolution (logMAR) was used as a measure of visual function. We included the visual function measurement only from patients where best correction was used (n=30).

Magnetic resonance imaging

Magnetic resonance imaging (MRI) was performed for all participants at 3T (MAGNETOM Trio Siemens, Erlangen, Germany) on the same day as the clinical examination, except for two participants, where there was an interval of one day. Details regarding the MRI protocol and the assessment of thalamic- and optic radiation lesions are given as supplementary material.

Measurement of thalamic volume and thalamic nuclei volume

The volumes of the entire thalamus and the thalamic nuclei were measured using the Multiple Automatically Generated Templates (MAGeT) brain algorithm [17]on 3D T1-weighted magnetization prepared rapid acquisition gradient echo (MPRAGE) images. MAGeT uses an atlas derived from manually segmented serial histological data, including delineation of the thalamic nuclei. It first customizes the atlas to a subset of participants, representative of the study population, using nonlinear registration and uses this newly segmented subset as a template library for the remaining participants. This has the advantage of correcting for the neuroanatomical variability of the study population. Details regarding the representative subset of the present study are given as supplementary material.

The segmentation results were visually inspected by one experienced rater (L.G.), who was blinded to the clinical data and no subjects had to be excluded. Last, all volumes were extracted and normalised using the SIENAX V-scaling factor for head-size[18]. Figure 1 and Supplementary figures 1 and 2 show examples of the LGN and VPN as segmented by MAGeT.

Mean upper cervical cord area

The mean upper cervical cord area (MUCCA) was used as a sensitive measure to assess spinal cord atrophy in patients with NMOSD[19]. Methodological details are given as supplementary material.

Optical coherence tomography

Retinal imaging was performed using a Heidelberg Engineering Spectralis spectral domain optical coherence tomography (OCT; Heidelberg Engineering, Heidelberg, Germany). We report the OCT acquisition settings, scanning protocol and details regarding excluded scans as supplementary material.

The peripapillary retinal nerve fiber layer (pRNFL) thickness and the combined ganglion cell and inner plexiform layer (GCIPL) volume were used in the analysis.

Statistical Analysis

Differences in age and sex-distribution between patients and controls were investigated using t-test and Fisher's exact test, respectively.

The associations of thalamic, LGN and VPN volumes with demographic characteristics were studied in controls using linear mixed effect models (LMM), with age, sex, handedness and brain side as fixed effects. If not stated otherwise, group comparisons, as well as structural-structural and structural-functional associations of thalamic nuclei were also performed using LMM, to account for intra-subject inter-side dependencies. Age and sex were always included as fixed effects in these models. The association of LGN volume with visual function was studied in LMM with monocular logMAR as dependent variable and LGN volume sum of both hemispheres as independent variable, since both LGN receive afferences from each eye. Relevant results were checked in additional LMM, adjusting for OR lesions and retinal damage (mean pRNFL thickness). We also performed analyses stratified for: i) ON (for LGN), ii) myelitis (for VPN), and iii)

brainstem attacks (for VPN). We report effect sizes from the LMM as marginal R^2 (mR^2), representing the variance explained by the fixed effects alone, and conditional R^2 (cR^2), representing the variance explained by both fixed and random effects.

Associations between LGN and VPN volumes with number of attacks and FSS were studied through Spearman correlation tests, due to the non-normal distribution of these variables (analysis per patient, using the volume sum of both hemispheres). Bilateral ON was counted as two episodes.

Last, we performed an exploratory analysis comparing all other thalamic nuclei between patients and controls, using LMM. This analysis was corrected for multiple comparisons using the Holm-Bonferroni method.

For all models, statistical significance was achieved at $p < 0.05$. All statistical analysis was performed using R[20], version 3.4.3 with packages: pastecs, lme4, lmerTest, MuMIn and ggplot2.

Data availability statement

All anonymised data not published within this article can be shared upon reasonable request from any qualified investigator.

RESULTS

Demographics, clinical and imaging characteristics of the study population

Patients with NMOSD and controls showed no difference regarding mean age (p=0.447), sex (p=0.475) or handedness (p=0.494; table 1).

Twenty-five patients (64.1%) had a history of at least one ON (NMO-ON) and the rest never had an ON (NMO-NON). Most patients (92.3%) had at least one myelitis, while there were also five patients with a brainstem attack (table 1).

A total of 17/39 (43.6%) patients had OR lesions, typically small, with nonspecific morphology (median lesion number: 0, range: 0-18). There was a single patient with a

left thalamic lesion. Since the left LGN and VPN volumes of this patient were not outliers (147.7 mm^3 and 612.2 mm^3, respectively) we did not exclude this patient from the analysis.

Volume of the entire thalamus

In controls, thalamic volume was associated with age (B=-17.50, SE=8.45, p=0.047) and brain side, with the thalamus being larger on the right (7760.5 ± 602.3 mm^3) compared to left (7185.7 ± 560.2 mm^3; B=573.54, SE=34.26, p<0.001).

Total thalamic volume did not differ between NMOSD patients (7382.6 ± 668.7 mm^3) and controls (7473.1 ± 646.1 mm^3), when accounting for age and brain side (B=-68.49, SE=119.62, p=0.569).

Volume of the LGN

In controls, LGN volume was also associated with brain side, with the LGN being larger on the right (240.3 ± 29.9 mm^3) compared to left (156.3 ± 20.6 mm^3; B=83.42, SE=3.53, p<0.001), but not with age, sex or handedness. Mean LGN volume did not differ between NMOSD patients and controls (table 2).

Table 2: Volumes of the lateral geniculate nucleus and ventral posterior nucleus in NMOSD patients and controls

	Controls (n=37)	**NMOSD (n=39)**	**NMO-ON (n=25)**	**NMO-NON (n=14)**	**NMOSD vs. controls**	**NMO-ON vs. controls**	**NMO-NON vs. controls**
LGN volume, mm^3	198.3 ± 49.4	190.4 ± 47.5	181.6 ± 44.2	206.1 ± 50	B= -9.38 (SE=5.23) p=0.077	**B= -16.97 (SE=5.65) p=0.004**	B= 5.31 (SE=7.49) p=0.483

(mean ± SD)							
	Controls (n=37)	**NMOSD (n=39)**	**NMOSD with myelitis (n=36)**	**NMOSD without myelitis (n=3)**	**NMOSD vs. controls**	**NMOSD with myelitis vs. controls**
VPN volume, mm^3 (mean ± SD)	679.7 ± 68.3	676.5 ± 67.8	674.3 ± 67.5	703.2 ± 71.7	B= -4.58 (SE=13.44) p=0.734	B= -7.36 (SE=13.75) p=0.594

Legend: Note that due to the fact that there were only three NMOSD patients without myelitis, we did not compare VPN volume between patients with and without myelitis. Abbreviations: LGN= lateral geniculate nucleus, NMOSD= neuromyelitis optica spectrum disorders, NMO-ON= patients with NMOSD and previous optic neuritis, NMO-NON= patients with NMOSD and negative history of previous ON, SE= standard error, VPN= ventral posterior nucleus mm^3

LGN volume was lower in NMO-ON patients compared to NMO-NON patients (B=-23.74, SE= 6.76, p=0.001, mR^2= 0.05, cR^2=0.94; Fig. 2) and in NMO-ON patients vs. controls (table 2, Fig. 2). These results remained after exclusion of seven patients on daily prednisolone (data not shown). In contrast, there was no difference between NMO-NON patients and controls (table 2, Fig. 2).

For a separate analysis of the ipsi- and contralateral LGN volumes and their association to ON, see supplementary material.

Volume of the LGN, optic neuritis and OCT parameters

In line with the smaller LGN found in NMO-ON, LGN volume inversely correlated with number of ON episodes in patients (Rho=-0.536, p<0.001; Fig. 2). When assuming a linear relationship, each ON episode led to, on average, an LGN volume loss of -3.09 mm^3 (SE=1.16, p=0.012). We did not find an association between LGN volume and time since first (B=-0.16, SE=0.67, p=0.809) or last ON episode (B= 1.28, SE= 1.29, p=0.33). In patients, LGN volume was associated with mean pRNFL thickness (B=0.70, SE=0.14, p<0.001, mR^2=0.07, cR^2=0.94) and mean GCIPL volume of both eyes (B=51.82, SE=11, p<0.001, mR^2=0.06, cR^2=0.94) (Fig. 2). The results were similar in models adjusted for OR lesions (pRNFL: B=0.71, SE=0.15, p<0.001; GCIPL: B=51.86, SE=11.10, p<0.001). In controls, there were no associations of pRNFL and GCIPL with LGN volume (data not shown).

When looking at NMO-NON and NMO-ON patients separately, the associations of LGN volume with pRNFL thickness and GCIPL volume remained only in the NMO-ON subgroup (pRNFL: B=0.64, SE=0.21, p=0.007, mR^2=0.05, cR^2=0.93; GCIPL: B=40.18, SE=16.18, p=0.023, mR^2=0.04, cR^2=0.93), but not in NMO-NON patients (pRNFL: B=0.19, SE=0.55, p=0.741; GCIPL: B=40.51, SE=39.09, p=0.322).

Volume of the LGN and lesions in the optic radiations

Presence of OR lesions was not associated with ipsilateral LGN volume (B=-0.52, SE= 6.35, p=0.935) and OR lesion number did not correlate with LGN volume (Rho=0.026, p=0.877). Moreover, LGN volume remained smaller in NMO-ON than in NMO-NON, when accounting for OR lesions (B=-23.74, SE= 6.82, p=0.001, mR^2= 0.05, cR^2=0.94).

Volume of the LGN and visual function

LGN volume (sum of both hemispheres) was associated with visual function measured as logMAR (B=-0.01, SE=0.002, p=0.002, mR^2=0.22, cR^2=0.27). This effect did not remain significant after inclusion of pRNFL thickness in the model (LGN: B=0.001, SE=0.002, p=0.613; pRNFL: B=-0.02, SE=0.003, p<0.001, mR^2=0.52, cR^2=0.52).

Volume of the VPN

In controls, VPN volume was associated with brain side, with the VPN being larger on the left (706.7 ± 65.8 mm^3) compared to right (652.8 ± 60.4 mm^3; B=-54.44, SE= 6.54, p<0.001), but not with age, sex or handedness.

Mean VPN volume was not different between NMOSD patients and controls (B=-4.58, SE=13.4, p=0.730; table 2 and Fig. 3).

Volume of the VPN and myelitis

There was no difference in VPN volume between patients with myelitis and controls (table 2). This remained after exclusion of seven patients on daily prednisolone (data not shown). Moreover, we found no correlation between VPN volume and number of myelitis episodes (Rho=-0.155, p=0.346; Fig. 3), time since first (B=-1.09, SE=1.48, p=0.466), or last myelitis (B=-4.32, SE= 2.78, p=0.131).

To study associations between VPN and myelitis-related spinal cord damage, we used the mean upper cervical cord area (MUCCA; mean in patients: 68.3 ± 7.0 mm^2 vs. 74.8 ± 6.4 mm^2 in controls). MUCCA was neither associated with VPN volume in NMOSD patients (B=-1.52, SE=1.33, p=0.261; Fig. 3) nor in the subgroup of patients with myelitis (B=-2.45, SE=1.37, p=0.084). Similar results were seen in controls (data not shown).

Moreover, there was no correlation between VPN volume and sensory FSS (Rho=-0.282, p=0.091).

Volume of the VPN and brainstem attacks

Due to the unexpected lack of association between VPN and myelitis, and since the VPN segmented in the present study included the ventral posterolateral nucleus, which receives afferences from the brainstem (trigeminothalamic tract), we performed a subgroup analysis in patients that had both myelitis and brainstem attacks (n=5; see table 3).

Table 3: Patients with myelitis and brainstem attacks

Patient	**First attack**	**Further attacks before study-baseline**	**Time since last brainstem attack**	**MRI at study-baseline**
1	Combined brainstem syndrome (double vision, nystagmus, tinnitus, headache, neck pain) and cervical myelitis (left hemiparesis)	Six episodes of myelitis (incl. cervical myelitis), no further brainstem attacks	20.9 years (last brainstem attack was the first attack)	LETM including the medulla and cervical spinal cord (to level C5)
2	Combined brainstem/ area postrema syndrome (double vision, nausea, vomiting, hiccups, dizziness) and cervical myelitis (sensory loss	One further attack: combined brainstem syndrome (dizziness, double vision, nystagmus) and cervical myelitis (right	3.66 years	LETM including the medulla and cervical spinal cord (to level C6)

	and dysaesthesias on the left)	hemiparesis and hemiataxia)		
3	Combined cervical myelitis (paresthesias on the left hemibody and spastic tetraparesis) with brainstem syndrome („brainstem encephalitis“; no further details available)	One further attack with nausea/vomiting and fatigue (probably brainstem/area postrema syndrome)	14.11 years	Lesions in the medulla and in the cervical spinal cord (level C5)
4	Combined brainstem syndrome (dizziness, nystagmus, balance problems, headache and neck pain) and cervical myelitis (sensory loss in four extremities and trunk)	Five episodes of optic neuritis and two of myelitis, no further brainstem attacks	6.66 years (last brainstem attack was the first attack)	LETM including the medulla and cervical spinal cord (to level C7)
5	Brainstem syndrome/area postrema (double vision, nausea, vomiting, dizziness)	One myelitis (one month after first attack), no further brainstem attacks	1.26 years (last brainstem attack was the first attack)	Multiple lesions in the medulla and cervical spinal cord, LETM in

				thoracic spinal cord (Th4-10)

Legend: The lesions in the medulla and spinal cord of these patients were identified by two raters: a board-certified neurologist with experience in neuroimaging (A.P.) and a board-certified radiologist (M.S.), on sagittal T2-weighted spinal cord MR images (repetition time (TR) = 3500 ms, echo time (TE) = 101 ms, in-plane resolution = 0.91 mm × 0.91 mm, slice thickness = 2 mm). Abbreviations: C= cervical, LETM=longitudinal extensive transverse myelitis, Th= thoracic

Indeed, we found lower VPN volumes in these patients (613.6 ± 71.8 mm^3) vs. controls (679.7 ± 68.33; B=-76.18, SE=30.52, p=0.017, mR^2=0.12, cR^2=0.85; Fig. 4). Since two of these patients were on daily prednisolone, we also performed this analysis including prednisolone treatment as random effect and the result remained (B=-70.84, SE=31.83, p=0.048). There was also a correlation between VPN volume and number of brainstem attacks (Rho=-0.378, p=0.018), but no significant correlation with brainstem FSS (Rho=-0.314, p=0.058).

Volumes of the other thalamic nuclei

In an exploratory analysis, we investigated whether other thalamic nuclei were different in NMOSD patients vs. controls. Among nine nuclei, we found only the lateral posterior nucleus to be smaller in patients (table 4). When corrected for multiple comparisons, this effect became non-significant (corrected p=0.180).

Table 4: Volumes of the remaining thalamic nuclei in NMOSD patients and controls

Volume of thalamic nuclei	NMOSD	Controls	Comparison
Medial geniculate nucleus (mm^3), mean ± SD	233.6 ± 34.1	233.2 ± 37.5	B=-0.49 (SE=5.18), p=0.925
Anterior nuclei (mm^3), mean ± SD	177.9 ± 41.9	189.4 ± 45.1	B=-11.69 (SE=6.32), p=0.068
Central nuclei (mm^3), mean ± SD	276.5 ± 60.2	273.1 ± 56.5	B=3.90 (SE=4.67), p=0.407
Lateral dorsal nucleus (mm^3), mean ± SD	66.4 ± 13.8	66.6 ± 7.7	B=-0.25 (SE=2.05), p=0.903
Lateral posterior nucleus (mm^3), mean ± SD	521.4 ± 77.2	547.0 ± 68.2	B=-27.1 (SE=11.34), p=0.020
Medial dorsal nucleus (mm^3), mean ± SD	1129.2 ± 186.1	1131.2 ± 376.6	B=3.43 (SE=32.77), p=0.917
Pulvinar (mm^3), mean ± SD	2022.0 ± 376.6	2028.4 ± 377.1	B=11.17 (SE=54.91), p=0.839
Ventral anterior nucleus (mm^3), mean ± SD	647.7 ± 95.4	670.6 ± 111.2	B=-22.32 (SE=14.19), p=0.120

Ventral lateral nucleus (mm^3), mean ± SD	1007.2 ± 114.5	1022.4 ± 97.7	B=-13.93 (SE=16.92), p=0.413

Legend: Note that all volumes are normalised using the SIENAX V-scaling factor and that the p-values given are uncorrected for multiple comparisons. After correction for multiple comparisons, the lateral posterior nucleus was not smaller in NMOSD than controls (corrected p=0.180). Abbreviations: SE= standard error.

DISCUSSION

In this study that assessed all thalamic nuclei in patients with NMOSD, we hypothesized that attack-related damage would be measurable as volume loss only in specific nuclei (LGN due to ON and VPN due to myelitis).

Indeed, LGN volume was reduced in NMOSD patients with ON history compared to controls, and also compared to patients without prior ON. Moreover, LGN volume was associated with number of ON episodes, retinal damage and visual function. These results strongly suggest anterograde degeneration in the afferent visual pathway of NMO-ON patients. Moreover, they support the use of LGN volume as an imaging marker of attack-related brain structural damage in NMOSD, with also functional relevance.

Anterograde degeneration in the visual pathway is well established in multiple sclerosis (MS) [21,22], while even in radiologically isolated syndrome there seems to be an association between retinal and thalamic volume loss[23]. In NMOSD, previous studies investigated transsynaptic degeneration in the visual pathway by analysing changes in the OR[15,24–27]. Several studies using diffusion tensor imaging [15,24,27,28] reported decreased OR fractional anisotropy, indicating microstructural OR-changes in NMO-ON patients vs. controls. A further study[25] showed reduced myelin water fraction,

suggesting reduced myelin density, in the OR of NMOSD patients (80% with prior ON) compared to controls. The interpretation of these findings was, that axonal loss in the optic nerve after ON can cause OR changes, by a propagation of damage through the LGN-synapses (anterograde transsynaptic degeneration).

However, reported microstructural damage in the OR of NMOSD patients *without* prior ON [26,27] suggests that white matter in this region might also be prone to direct changes due to NMOSD-related astrocytopathy. Thus, the specific assessment of the LGN, the grey matter structure where the actual synapses occur, is crucial to confirm transsynaptic degeneration and measure attack-related structural damage in the visual pathway in NMOSD. Moreover, LGN volume as assessed in our study has the advantage of using a broadly available MRI sequence (3D T1-weighted). This is important, since standardized diffusion tensor imaging for the OR-assessment is often hampered in clinical routine.

The lack of data on LGN volume in NMOSD is probably due to the small LGN size, which makes its measurement technically challenging[22]. A single previous study[27] reported, in line with our results, reduced LGN volume in NMOSD patients with ON compared to controls and to patients without ON. In this previous study however, LGN volume was measured manually, which is prone to bias, especially for such a small structure[29]. In the present study, we used a multi-atlas-based tool of automated segmentation, the MAGeT Brain algorithm[17]. This algorithm is based on histological data, was validated against manual segmentations[30,31] and intraoperative recordings[31] and was previously used to investigate deep grey matter volume in patients with MS[29].

Next to this methodological strength, the present study included a –given the rarity of NMOSD in Europe[32]- relatively large (n=39) number of AQP4-IgG seropositive

NMOSD patients, compared to the heterogeneous population of Tian et al.[27], who analysed AQP4-IgG seropositive and seronegative patients together, and to the smaller sampler sizes of previous studies investigating the visual pathway of AQP4-IgG seropositive NMOSD[15,24–26].

Although previous work showed GCIPL volume reduction[6] and microstructural OR changes[26] in AQP4-IgG seropositive NMO-NON patients, our current results do not support a subclinical LGN volume loss in the absence of ON, since NMO-NON patients had normal LGN volumes. The reasons for this are not clear. It could be that neurodegenerative processes are different in the retina than the brain and in the white- than the grey matter in NMOSD. However, it cannot be ruled out that in this cross-sectional study we had insufficient power to detect subtle subclinical volume loss at the LGN level.

The LGN volume was not associated with OR lesions in our study. This is in contrast to what was shown in MS[33], where findings suggest retrograde degeneration from OR lesions towards the retina[34]. The reason for this could be, that the typically small, nonspecific lesions observed in the OR of NMOSD patients are less destructive than demyelinating OR lesions in MS. This would be in line with the nonspecific morphology and asymptomatic nature of most white matter brain lesions in NMOSD[35–37].

In contrast to the LGN findings, VPN volume was not smaller in NMOSD patients with myelitis vs. controls and did not correlate with number of myelitis episodes. One possible explanation for these negative findings is, that compared to the small LGN, which receives afferences almost exclusively from the retina/optic nerve, the VPN is a larger nuclear complex receiving afferences from several regions [38]. Moreover, the VPN as segmented in the present study included not only the ventral posterolateral subnucleus (receiving afferences from the spinal cord), but also the ventral intermediate nucleus and

the ventral posteromedial subnucleus. The latter receives afferences from the trigeminothalamic tract in the brainstem[39]. Accordingly, we found reduced VPN volumes in five patients who suffered brainstem relapses. Four of these patients had attacks with brainstem or area postrema syndromes and cervical myelitis, with MRI lesions extending from the brainstem into the cervical spinal cord. We speculate that a lesion located in the most cranial part of the spinal cord (i.e. a shorter distance from the VPN) and the brainstem (i.e. close to the spinal tract of the trigeminal nerve and/or the trigeminothalamic tract) might be associated with the VPN volume loss seen in these patients.

Another possible explanation for the lack of association between VPN and myelitis is the heterogeneous population of patients, with different degrees of sensory involvement, as well as spinal cord lesions with different lengths and locations. Last, it should be emphasized that lack of volume loss in the VPN does not necessarily mean lack of damage. Microstructural changes that do not necessarily result in a volume reduction or functional, adaptive changes could be present in the grey matter, despite “normal” volume.

The volume of the entire thalamus was not reduced in our NMOSD patients compared to controls, which is in line with three previous European studies[13–15] with AQP4-IgG seropositive patients. However, three other Asian studies[11,12,16] reported reduced thalamic volumes compared to controls. In one of these studies[12], seven thalamic subregions (not corresponding to specific subnuclei) were also examined separately and almost all showed reduced volumes in NMOSD. These overall conflicting findings may be due to the genetically different NMOSD populations in Europe and Asia[40] and due to variability in antibody-status of the patients, with the Asian studies including also 10-30% AQP4-IgG seronegative patients[11,12,16].

A limitation of our study is the use of volume changes as the only measure of thalamic damage. Quantitative imaging methods, such as diffusion tensor imaging of thalamic nuclei, or even functional MRI might contribute to our understanding of microstructural and functional changes in NMOSD that do not necessarily result in volume loss, although their application in such small structures as the thalamic nuclei would be technically challenging. Moreover, the cross-sectional nature of the present study is a drawback. Longitudinal studies following changes in thalamic nuclei in patients with NMOSD after an acute (ideally the first) attack would be warranted in the future.

To conclude, we found structural damage of the LGN due to ON in AQP-IgG seropositive NMOSD patients. Our results support the role of this thalamic nucleus as an imaging marker of attack-related neurodegenerative damage in the brain of these patients, also with functional relevance (association with visual function). Similar results were not observed for VPN and myelitis, although we saw an association with brainstem attacks, which needs confirmation in larger studies. Our findings suggest selective, attack-related rather than diffuse damage to thalamic nuclei in NMOSD.

ACKNOWLEDGMENTS

We thank all patients and controls that participated in this study, Charlotte Bereuter for performing the visual assessment and optical coherence tomography, as well as Susan Pikol and Cynthia Kraut for performing the magnetic resonance imaging.

FUNDING

This study was supported by the “Deutsche Forschungsgemeinschaft” (grant DFG Exc. 257) and the German Federal Ministry for Education and Research (BMBF; grant N2-ADVISIMS: 16GW0079) to F.P. and A.U.B. and by the Swiss National Science Foundation (project number P300PB_174480) to A.P.

COMPETING INTERESTS

Athina Papadopoulou has received speaker-fee from Sanofi-Genzyme and travel support from Bayer AG, Teva and Hoffmann-La Roche. Her research was supported by the University of Basel, the Swiss Multiple Sclerosis Society and the "Stiftung zur Förderung der gastroenterologischen und allgemeinen klinischen Forschung sowie der medizinischen Bildauswertung". The current research work was supported by the Swiss National Science Foundation (Project number: P300PB_174480).

Frederike Cosima Oertel was employee of Nocturne UG, not in context of this work.

Laura Gaetano was a temporary employee of Novartis AG and is currently an employee of Hoffmann-La Roche; her contribution to this work was prior to her employment in Hoffmann-La Roche.

Joseph Kuchling received conference registration fees from Biogen and financial research support from Krankheitsbezogenes Kompetenznetzwerk Multiple Sklerose (KKNMS).

Hanna Zimmermann received research grants from Novartis and speaker fees from Teva.

Claudia Chien has nothing to disclose.

Nadja Siebert has nothing to disclose.

Susanna E. Asseyer has nothing to disclose.

Judith Bellmann-Strobl has received travel grants and speaking fees from Bayer Healthcare, Biogen Idec, Merck Serono, Sanofi-Aventis/Genzyme, Teva Pharmaceuticals, and Novartis.

Klemens Ruprecht served on the scientific advisory board for Sanofi-Aventis/Genzyme, Novartis, and Roche; received travel funding and/or speaker honoraria from Bayer Healthcare, Biogen Idec, Merck Serono, Sanofi-Aventis/Genzyme, Teva Pharmaceuticals, Novartis, and Guthy Jackson Charitable Foundation; is an academic

editor for PLoS ONE; receives publishing royalties from Elsevier; and received research support from Novartis and German Ministry of Education and Research.

Mallar M. Chakravarty has nothing to disclose.

Michael Scheel has nothing to disclose.

Stefano Magon has received research support from Swiss MS Society, Swiss National Science Foundation, University of Basel and Stiftung zur Förderung der gastroenterologischen und allgemeinen klinischen Forschung sowie der medizinischen Bildauswertung University Hospital Basel. He also received travel support from Biogen and Genzyme.

Jens Wuerfel is CEO of MIAC AG Basel, Switzerland. He served on scientific advisory boards of Actelion, Biogen, Genzyme-Sanofi, Novartis, and Roche. He is or was supported by grants of the EU (Horizon2020), German Federal Ministeries of Education and Research (BMBF) and of Economic Affairs and Energy (BMWI).

Friedemann Paul serves on the scientific advisory board for Novartis; received speaker honoraria and travel funding from Bayer, Novartis, Biogen Idec, Teva, Sanofi-Aventis/Genzyme, Merck Serono, Alexion, Chugai, MedImmune, and Shire; is an academic editor for PLoS ONE; is an associate editor for Neurology® Neuroimmunology & Neuroinflammation; consulted for SanofiGenzyme, Biogen Idec, MedImmune, Shire, and Alexion; and received research support from Bayer, Novartis, Biogen Idec, Teva, Sanofi-Aventis/Genzyme, Alexion, Merck Serono, German Research Council, Werth Stiftung of the City of Cologne, German Ministry of Education and Research, Arthur Arnstein Stiftung Berlin, EU FP7 Framework Program, Arthur Arnstein Founda-tion Berlin, Guthy Jackson Charitable Foundation, and National Multiple Sclerosis of the USA.

Alexander U. Brandt is cofounder and shareholder of technology startups Motognosis and Nocturne UG. He is named as inventor on several patent applications describing MS serum biomarkers, perceptive visual computing and retinal image analysis.

AUTHORS CONTRIBUTORSHIP:

Conception and design of the study: A.P. and A.U.B.

Acquisition, analysis & interpretation of data: AP. F.C.O., L.G., J.K., H.G.Z., C.C., N.S., S.E.A., J.B.S., K.R., M.M. Ch., M.Sch., S.M., J.W., F.P., and A.U.B.

Drafting the manuscript or figures: A.P., F.C.O., J.K., H.G.Z., C.C., N.S., M.M. Ch., S.M., J.W., F.P. and A.U.B.

REFERENCES

1 Wingerchuk DM, Banwell B, Bennett JL, *et al.* International consensus diagnostic criteria for neuromyelitis optica spectrum disorders. *Neurology* 2015;**85**:177–89. doi:10.1212/WNL.0000000000001729

2 Jacob A, McKeon A, Nakashima I, *et al.* Current concept of neuromyelitis optica (NMO) and NMO spectrum disorders. *J Neurol Neurosurg Psychiatry* 2013;**84**:922–30. doi:10.1136/jnnp-2012-302310

3 Wingerchuk DM, Pittock SJ, Lucchinetti CF, *et al.* A secondary progressive clinical course is uncommon in neuromyelitis optica. *Neurology* 2007;**68**:603–5. doi:10.1212/01.wnl.0000254502.87233.9a

4 Kitley J, Leite MI, Nakashima I, *et al.* Prognostic factors and disease course in aquaporin-4 antibody-positive patients with neuromyelitis optica spectrum disorder from the United Kingdom and Japan. *Brain J Neurol* 2012;**135**:1834–49. doi:10.1093/brain/aws109

5 Bonnan M, Valentino R, Debeugny S, *et al.* Short delay to initiate plasma exchange is the strongest predictor of outcome in severe attacks of NMO spectrum disorders. *J Neurol Neurosurg Psychiatry* 2018;**89**:346–51. doi:10.1136/jnnp-2017-316286

6 Oertel FC, Havla J, Roca-Fernández A, *et al.* Retinal ganglion cell loss in neuromyelitis optica: a longitudinal study. *J Neurol Neurosurg Psychiatry* 2018;**89**:1259–65. doi:10.1136/jnnp-2018-318382

7 Rocca MA, Agosta F, Mezzapesa DM, *et al.* Magnetization transfer and diffusion tensor MRI show gray matter damage in neuromyelitis optica. *Neurology* 2004;**62**:476–8.

8 Yu CS, Lin FC, Li KC, *et al.* Diffusion tensor imaging in the assessment of normal-appearing brain tissue damage in relapsing neuromyelitis optica. *AJNR Am J Neuroradiol* 2006;**27**:1009–15.

9 Kawachi I, Lassmann H. Neurodegeneration in multiple sclerosis and neuromyelitis optica. *J Neurol Neurosurg Psychiatry* 2017;**88**:137–45. doi:10.1136/jnnp-2016-313300

10 Saji E, Arakawa M, Yanagawa K, *et al.* Cognitive impairment and cortical degeneration in neuromyelitis optica. *Ann Neurol* 2013;**73**:65–76. doi:10.1002/ana.23721

11 Liu Y, Fu Y, Schoonheim MM, *et al.* Structural MRI substrates of cognitive impairment in neuromyelitis optica. *Neurology* 2015;**85**:1491–9. doi:10.1212/WNL.0000000000002067

12 Liu Y, Duan Y, Huang J, *et al.* Multimodal Quantitative MR Imaging of the Thalamus in Multiple Sclerosis and Neuromyelitis Optica. *Radiology* 2015;**277**:784–92. doi:10.1148/radiol.2015142786

13 Matthews L, Kolind S, Brazier A, *et al.* Imaging Surrogates of Disease Activity in Neuromyelitis Optica Allow Distinction from Multiple Sclerosis. *PloS One* 2015;**10**:e0137715. doi:10.1371/journal.pone.0137715

14 Finke C, Heine J, Pache F, *et al.* Normal volumes and microstructural integrity of deep gray matter structures in AQP4+ NMOSD. *Neurol Neuroimmunol Neuroinflammation* 2016;**3**:e229. doi:10.1212/NXI.0000000000000229

15 Pache F, Zimmermann H, Finke C, *et al.* Brain parenchymal damage in neuromyelitis optica spectrum disorder - A multimodal MRI study. *Eur Radiol* 2016;**26**:4413–22. doi:10.1007/s00330-016-4282-x

16 Hyun J-W, Park G, Kwak K, *et al.* Deep gray matter atrophy in neuromyelitis optica spectrum disorder and multiple sclerosis. *Eur J Neurol* 2017;**24**:437–45. doi:10.1111/ene.13224

17 Chakravarty MM, Steadman P, van Eede MC, *et al.* Performing label-fusion-based segmentation using multiple automatically generated templates. *Hum Brain Mapp* 2013;**34**:2635–54. doi:10.1002/hbm.22092

18 Smith SM, Zhang Y, Jenkinson M, *et al.* Accurate, robust, and automated longitudinal and cross-sectional brain change analysis. *NeuroImage* 2002;**17**:479–89.

19 Chien C, Scheel M, Schmitz-Hübsch T, *et al.* Spinal cord lesions and atrophy in NMOSD with AQP4-IgG and MOG-IgG associated autoimmunity. *Mult Scler Houndmills Basingstoke Engl* 2018;:1352458518815596. doi:10.1177/1352458518815596

20 R Core Team (2017). R: A language and environment for statistical computing. R Foundation for Statistical Computing, Vienna, Austria. https://www.r-project.org/ (accessed 23 Nov 2018).

21 Balk LJ, Steenwijk MD, Tewarie P, *et al.* Bidirectional trans-synaptic axonal degeneration in the visual pathway in multiple sclerosis. *J Neurol Neurosurg Psychiatry* 2015;**86**:419–24. doi:10.1136/jnnp-2014-308189

22 Gabilondo I, Martínez-Lapiscina EH, Martínez-Heras E, *et al.* Trans-synaptic axonal degeneration in the visual pathway in multiple sclerosis. *Ann Neurol* 2014;**75**:98–107. doi:10.1002/ana.24030

23 Vural A, Okar S, Kurne A, *et al.* Retinal degeneration is associated with brain volume reduction and prognosis in radiologically isolated syndrome. *Mult Scler Houndmills Basingstoke Engl* 2018;:1352458518817987. doi:10.1177/1352458518817987

24 Pichiecchio A, Tavazzi E, Poloni G, *et al.* Advanced magnetic resonance imaging of neuromyelitis optica: a multiparametric approach. *Mult Scler Houndmills Basingstoke Engl* 2012;**18**:817–24. doi:10.1177/1352458511431072

25 Manogaran P, Vavasour IM, Lange AP, *et al.* Quantifying visual pathway axonal and myelin loss in multiple sclerosis and neuromyelitis optica. *NeuroImage Clin* 2016;**11**:743–50. doi:10.1016/j.nicl.2016.05.014

26 Oertel FC, Kuchling J, Zimmermann H, *et al.* Microstructural visual system changes in AQP4-antibody-seropositive NMOSD. *Neurol Neuroimmunol Neuroinflammation* 2017;**4**:e334. doi:10.1212/NXI.0000000000000334

27 Tian D-C, Su L, Fan M, *et al.* Bidirectional degeneration in the visual pathway in neuromyelitis optica spectrum disorder (NMOSD). *Mult Scler Houndmills Basingstoke Engl* 2017;:1352458517727604. doi:10.1177/1352458517727604

28 Kuchling J, Backner Y, Oertel FC, *et al.* Comparison of probabilistic tractography and tract-based spatial statistics for assessing optic radiation damage in patients with autoimmune inflammatory disorders of the central nervous system. *NeuroImage Clin* 2018;**19**:538–50. doi:10.1016/j.nicl.2018.05.004

29 Magon S, Chakravarty MM, Amann M, *et al.* Label-fusion-segmentation and deformation-based shape analysis of deep gray matter in multiple sclerosis: the impact of thalamic subnuclei on disability. *Hum Brain Mapp* 2014;**35**:4193–203. doi:10.1002/hbm.22470

30 Chakravarty MM, Sadikot AF, Germann J, *et al.* Comparison of piece-wise linear, linear, and nonlinear atlas-to-patient warping techniques: analysis of the labeling of subcortical nuclei for functional neurosurgical applications. *Hum Brain Mapp* 2009;**30**:3574–95. doi:10.1002/hbm.20780

31 Chakravarty MM, Sadikot AF, Germann J, *et al.* Towards a validation of atlas warping techniques. *Med Image Anal* 2008;**12**:713–26. doi:10.1016/j.media.2008.04.003

32 Mori M, Kuwabara S, Paul F. Worldwide prevalence of neuromyelitis optica spectrum disorders. *J Neurol Neurosurg Psychiatry* 2018;**89**:555–6. doi:10.1136/jnnp-2017-317566

33 Sepulcre J, Goñi J, Masdeu JC, *et al.* Contribution of white matter lesions to gray matter atrophy in multiple sclerosis: evidence from voxel-based analysis of T1 lesions in the visual pathway. *Arch Neurol* 2009;**66**:173–9. doi:10.1001/archneurol.2008.562

34 Klistorner A, Sriram P, Vootakuru N, *et al.* Axonal loss of retinal neurons in multiple sclerosis associated with optic radiation lesions. *Neurology* 2014;**82**:2165–72. doi:10.1212/WNL.0000000000000522

35 Cabrera-Gómez JA, Quevedo-Sotolongo L, González-Quevedo A, *et al.* Brain magnetic resonance imaging findings in relapsing neuromyelitis optica. *Mult Scler Houndmills Basingstoke Engl* 2007;**13**:186–92. doi:10.1177/1352458506070725

36 Sinnecker T, Dörr J, Pfueller CF, *et al.* Distinct lesion morphology at 7-T MRI differentiates neuromyelitis optica from multiple sclerosis. *Neurology* 2012;**79**:708–14. doi:10.1212/WNL.0b013e3182648bc8

37 Matthews L, Marasco R, Jenkinson M, *et al.* Distinction of seropositive NMO spectrum disorder and MS brain lesion distribution. *Neurology* 2013;**80**:1330–7. doi:10.1212/WNL.0b013e3182887957

38 Kipp M, Wagenknecht N, Beyer C, *et al.* Thalamus pathology in multiple sclerosis: from biology to clinical application. *Cell Mol Life Sci CMLS* 2015;**72**:1127–47. doi:10.1007/s00018-014-1787-9

39 Kiernan, J., Rajakumar, R. *Barr's the human nervous system: an anatomical viewpoint*. 10th ed. Lippincott Williams & Wilkins 2013.

40 Kim S-H, Mealy MA, Levy M, *et al.* Racial differences in neuromyelitis optica spectrum disorder. *Neurology* Published Online First: 26 October 2018. doi:10.1212/WNL.0000000000006574

FIGURE LEGENDS

Figure 1: Lateral geniculate and ventral posterior nuclei and their afferences in the visual and sensory pathways.

A: The afferent visual pathway; note the LGN, which receives afferences from both optic nerves. We hypothesized LGN volume loss in NMOSD, due to optic neuritis. B: Axial T1-weighted 3D MPRAGE image showing an actual example of LGN segmentation (red) using the MAGeT brain algorithm in a control. Note also the optic tract in yellow. C: The thalamic VPN receives affereces from the spinothalamic pathway (in red) and dorsal column/medial lemniscal pathway (in green). We hypothesized VPN volume loss in NMOSD, due to myelitis involving these pathways. D: Coronal T1-weighted 3D MPRAGE image showing an actual example of VPN segmentation (turqoise) using the MAGeT brain algorithm in a control.

The Schematic Figure of the Afferent Visual System (A) is adapted from the website of the Neurodiagnostics Laboratory @ Charité – Universitätsmedizin Berlin, Germany (http://neurodial.de/2017/08/25/schematic-figure-the-afferent-visual-system-creative-commons-license).

Figure 2: Volume of the lateral geniculate nucleus in NMOSD and its relationship with optic neuritis and retinal axonal damage.

A: Normalized LGN volume per participant (mean of both hemispheres) in the three groups: controls in white, patients with NMOSD and negative ON history (NMO-NON) in light blue and patients with NMOSD and positive ON history (NMO-ON) in dark blue. B-C: Relationship between normalized LGN volume in NMOSD patients (sum of both hemispheres per patient) and: B) number of optic neuritis (ON) episodes, C) mean peripapillary retinal nerve fiber (pRNFL) thickness of both eyes.

Figure 3: Volume of the ventral posterior nucleus in NMOSD and its relationship with myelitis and spinal cord damage.

A: Normalized volume of the ventral posterior nucleus (VPN; in mm^3) per participant (mean of both hemispheres) in the three groups: controls in white, patients with NMOSD and myelitis in light blue and patients with NMOSD without myelitis in dark blue. No comparison was made between patients with- and without myelitis, due to the low number of the latter (n=3). B-C: Relationship between normalized VPN volume in NMOSD patients (sum of both hemispheres per patient) and: B) number of myelitis episodes, C) mean upper cervical cord area (MUCCA).

Figure 4: Volume of the ventral posterior nucleus in patients with myelitis and brainstem involvement.

Normalized volume of the ventral posterior nucleus (VPN) per participant (mean of both hemispheres) in the groups: controls in white and patients with NMOSD, myelitis and brainstem relapses in light blue ("NMO-brainstem").

3.

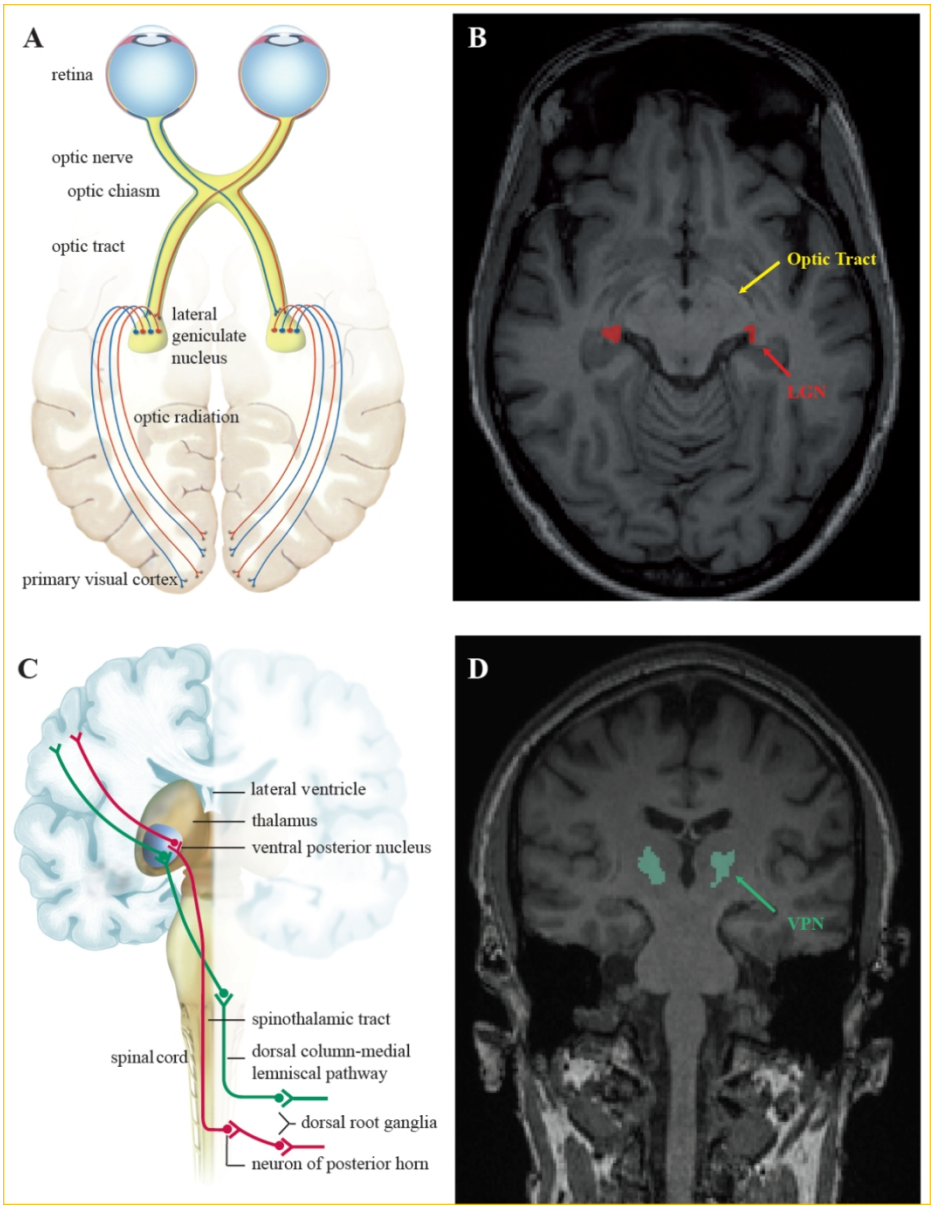

Lateral geniculate and ventral posterior nuclei and their afferences in the visual and sensory pathways.

103x133mm (300 x 300 DPI)

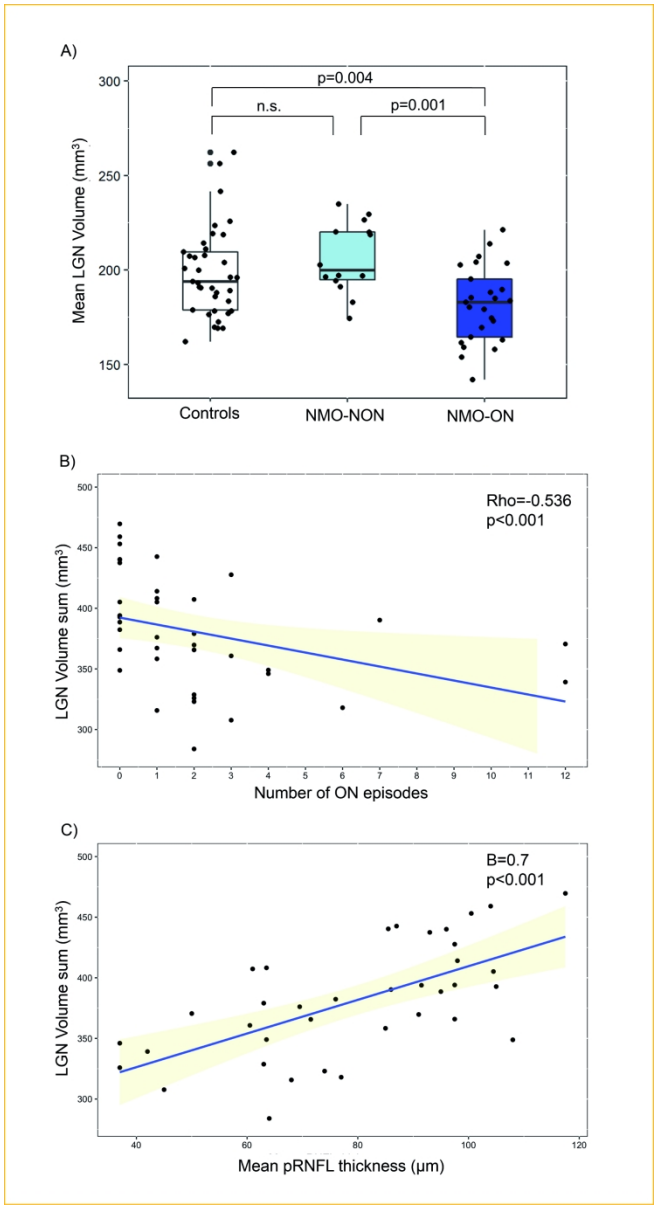

Volume of the lateral geniculate nucleus in NMOSD and its relationship with optic neuritis and retinal axonal damage.

159x294mm (300 x 300 DPI)

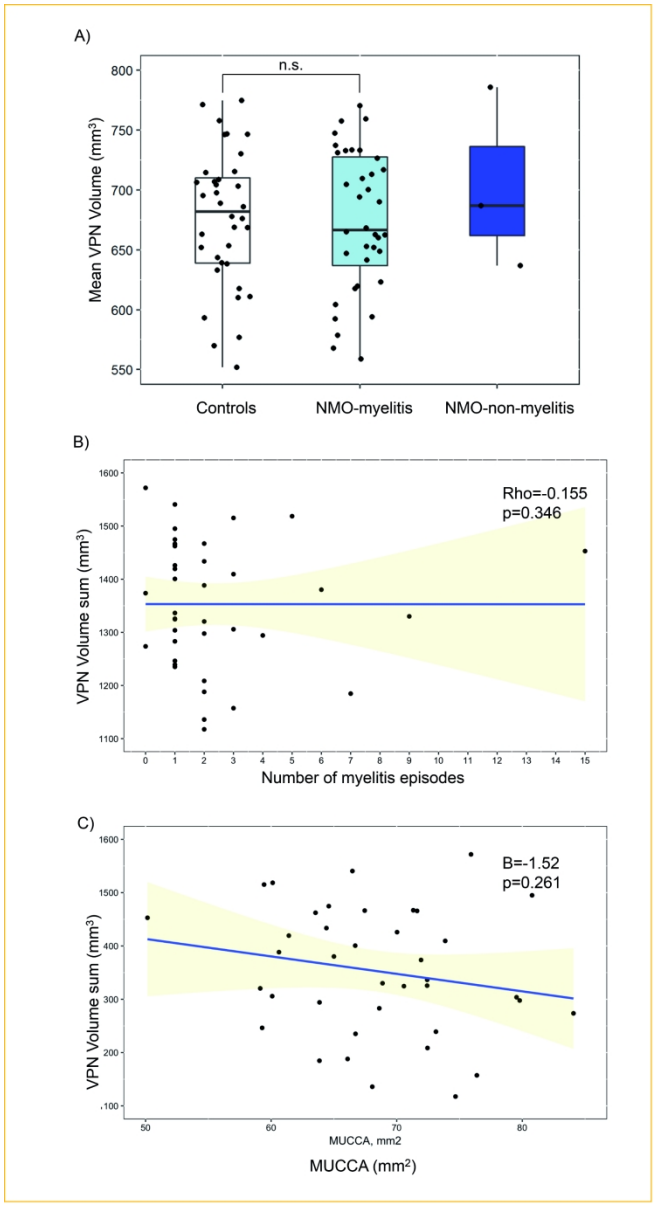

Volume of the ventral posterior nucleus in NMOSD and its relationship with myelitis and spinal cord damage.

159x294mm (300 x 300 DPI)

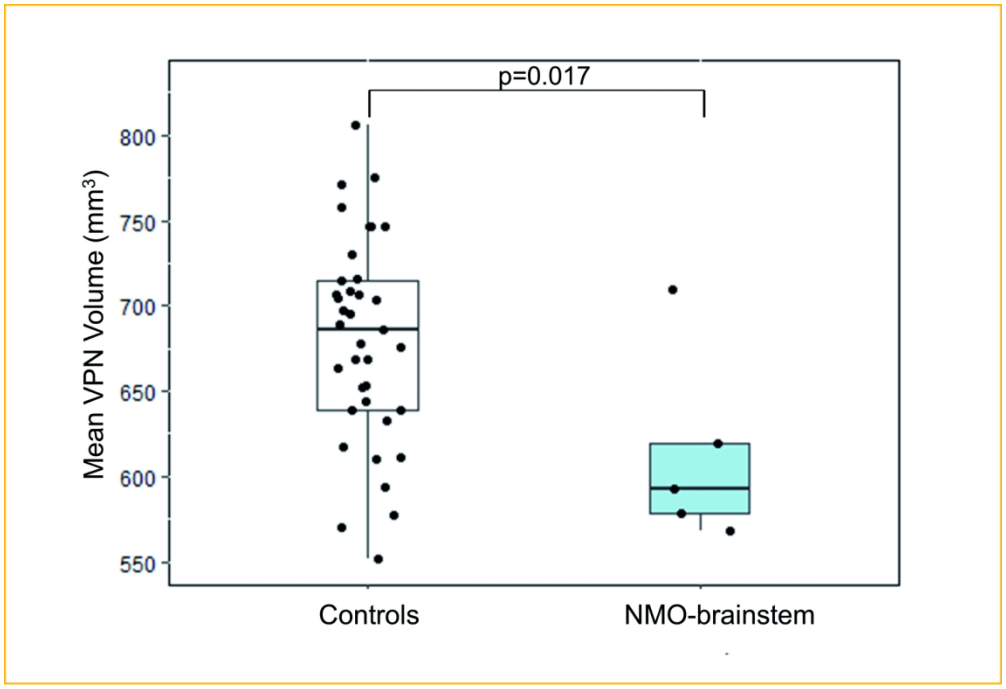

Volume of the ventral posterior nucleus in patients with myelitis and brainstem involvement.

159x108mm (300 x 300 DPI)

SUPPLEMENTARY MATERIAL

METHODS

Magnetic resonance imaging protocol

Magnetic resonance imaging (MRI) was performed for all subjects at 3T (MAGNETOM Trio Siemens, Erlangen, Germany). The protocol included a 3D T1-weighted magnetization prepared rapid acquisition gradient echo (MPRAGE) sequence (repetition time (TR) =1900 ms, echo time (TE) =3.03 ms, isotropic resolution 1x1x1 mm), and a 3D T2-weighted fluid-attenuated inversion recovery (FLAIR) sequence (TR = 6000 ms, TE = 388 ms, isotropic resolution 1x1x1 mm) of the brain.

Measurement of thalamic volume and thalamic nuclei volume using the MAGeT brain algorithm

The Multiple Automatically Generated Templates (MAGeT) brain algorithm [1,2] was used to segment the entire thalami and the different thalamic nuclei on MPRAGE MR images. MAGeT uses an atlas derived from manually segmented serial histological data, containing delineation of the thalamic nuclei, as per Hirai and Jones [3]. It first customizes the atlas to a subset of participants, representative of the entire study population, using a nonlinear registration scheme.

In our study, this representative subset was chosen in a manner consistent with best practices for the algorithm [4], according to age, sex and - for patients - number and type of attacks. It consisted of eleven NMOSD patients (ten women, mean age: 50±15.1 years, median number of attacks 3 (range 1-11), 10/11 with myelitis and 7/11 with ON) and ten controls (9 women, mean age: 47.4±12 years). This newly segmented subset acted as a template library for the remaining participants, to correct for the neuroanatomical variability of our study population and to average different sources of random error prior to the final segmentation [5].

Lesions in the thalamus and the optic radiations

The 3D T2-weighted fluid-attenuated inversion recovery (FLAIR) images of patients were assessed and verified for thalamic- and optic radiations (OR) lesions in consensus by a board-certified neurologist (A.P.) and a board-certified radiologist (M.S.), to assess whether lesions in these strategic locations may influence our results.

Mean upper cervical cord area

The mean upper cervical cord area (MUCCA) was used as a sensitive measure to assess spinal cord atrophy in patients with NMOSD[6]. MUCCA was measured in 3D MPRAGE images using an active surface model[7] by averaging the cross-sectional areas from five consecutive slices at the C2/C3 intervertebral space level, as described previously[6,8].

Optical coherence tomography: excluded scans and scanning protocol

Retinal imaging was performed using a Heidelberg Engineering Spectralis spectral domain optical coherence tomography (OCT; Heidelberg Engineering, Heidelberg, Germany), with ART (automatic real-time) function for image averaging. We did not use pupil dilation. All patients had the OCT on the same day as the MRI and clinical examination, except for two, where there was an interval of one day. For the controls there was often an interval of few days between OCT and MRI/clinical assessment (on average: 7.4±11.7 days, range 0-50 days).

A total of ten eyes from eight patients had to be excluded from the analysis: six eyes due to incidental findings, three due to lack of OCT data, and one due to quality reasons, according to the OSCAR-IB criteria. For two additional eyes, only the macular scan had to be excluded, due to quality reasons[9].

The OCT acquisition settings and scanning protocol are reported below, according to the APOSTEL recommendations [10]:

The peripapillary retinal nerve fiber layer (pRNFL) was measured using 3.4-mm ring scans around the optic nerve head (12°, 1536 A-scans, 9≤ ART ≤100). The combined ganglion cell and inner plexiform layer (GCIPL) volume was measured using a 6-mm diameter cylinder around the fovea from a macular volume scan (25°x30°, 61 vertical B-scans, 768 A-scans per B-scan, ART=15). Segmentation of the pRNFL and the intraretinal layers in the macular scan was performed semi-automatically using software provided by the optical coherence tomography manufacturer (Eye Explorer 1.9.10.0 with viewing module 6.0.9.0; Heidelberg Engineering). All measurements were checked for segmentation errors and corrected if necessary, by one experienced rater (F.C.O.).

RESULTS

Volume of the LGN: differences between ipsilateral and contralateral side to optic neuritis (ON)

Since the LGN of both hemispheres receive afferences from each optic nerve, both LGN were expected to be affected similarly after a unilateral ON episode.

To confirm this, we performed an additional analysis comparing the LGN volume between patients with ON (NMO-ON) and without ON (NMO-NON) separately for unilateral LGN to ON and contralateral LGN to ON. From this analysis, 12 NMO-ON patients with bilateral ON were excluded. From the included NMO-ON patients (n=13), 6 patients had ON on the left eye and 7 patients on the right eye. The NMO-NON patients were 14.

This analysis was performed using linear mixed effect models (LMM), with LGN volume being the dependent variable, ON history fixed effect, next to age and sex, and subject and side random effects.

Although the volume of ipsilateral to ON LGN was smaller than the LGN volume of NMO-NON patients (B=-21.10, SE= 8.69, p= 0.023, mR2= 0.05, cR2= 0.94), this was not the case for contralateral LGN to ON (B= -16.29, SE= 7.99, p= 0.052, mR2= 0.02, cR2=0.95).

However, the latter was a borderline not significant result, the p value being 0.052, and could be also due to the lower power of this subgroup analysis, which included a total of 41 LGN.

REFERENCES

1 Chakravarty MM, Bertrand G, Hodge CP, *et al.* The creation of a brain atlas for image guided neurosurgery using serial histological data. *NeuroImage* 2006;**30**:359–76. doi:10.1016/j.neuroimage.2005.09.041

2 Chakravarty MM, Steadman P, van Eede MC, *et al.* Performing label-fusion-based segmentation using multiple automatically generated templates. *Hum Brain Mapp* 2013;**34**:2635–54. doi:10.1002/hbm.22092

3 Hirai T, Jones EG. A new parcellation of the human thalamus on the basis of histochemical staining. *Brain Res Brain Res Rev* 1989;**14**:1–34.

4 Pipitone J, Park MTM, Winterburn J, *et al.* Multi-atlas segmentation of the whole hippocampus and subfields using multiple automatically generated templates. *NeuroImage* 2014;**101**:494–512. doi:10.1016/j.neuroimage.2014.04.054

5 Magon S, Chakravarty MM, Amann M, *et al.* Label-fusion-segmentation and deformation-based shape analysis of deep gray matter in multiple sclerosis: the impact of thalamic subnuclei on disability. *Hum Brain Mapp* 2014;**35**:4193–203. doi:10.1002/hbm.22470

6 Chien C, Scheel M, Schmitz-Hübsch T, *et al.* Spinal cord lesions and atrophy in NMOSD with AQP4-IgG and MOG-IgG associated autoimmunity. *Mult Scler Houndmills Basingstoke Engl* 2018;:1352458518815596. doi:10.1177/1352458518815596

7 Horsfield MA, Sala S, Neema M, *et al.* Rapid semi-automatic segmentation of the spinal cord from magnetic resonance images: application in multiple sclerosis. *NeuroImage* 2010;**50**:446–55. doi:10.1016/j.neuroimage.2009.12.121

8 Losseff NA, Webb SL, O'Riordan JI, *et al.* Spinal cord atrophy and disability in multiple sclerosis. A new reproducible and sensitive MRI method with potential to monitor disease progression. *Brain J Neurol* 1996;**119 (Pt 3)**:701–8.

9 Tewarie P, Balk L, Costello F, *et al.* The OSCAR-IB consensus criteria for retinal OCT quality assessment. *PloS One* 2012;**7**:e34823. doi:10.1371/journal.pone.0034823

10 Cruz-Herranz A, Balk LJ, Oberwahrenbrock T, *et al.* The APOSTEL recommendations for reporting quantitative optical coherence tomography studies. *Neurology* 2016;**86**:2303–9. doi:10.1212/WNL.0000000000002774

SUPPLEMENTARY FIGURES

Supplementary Figure 1: LGN segmentation by MAGeT

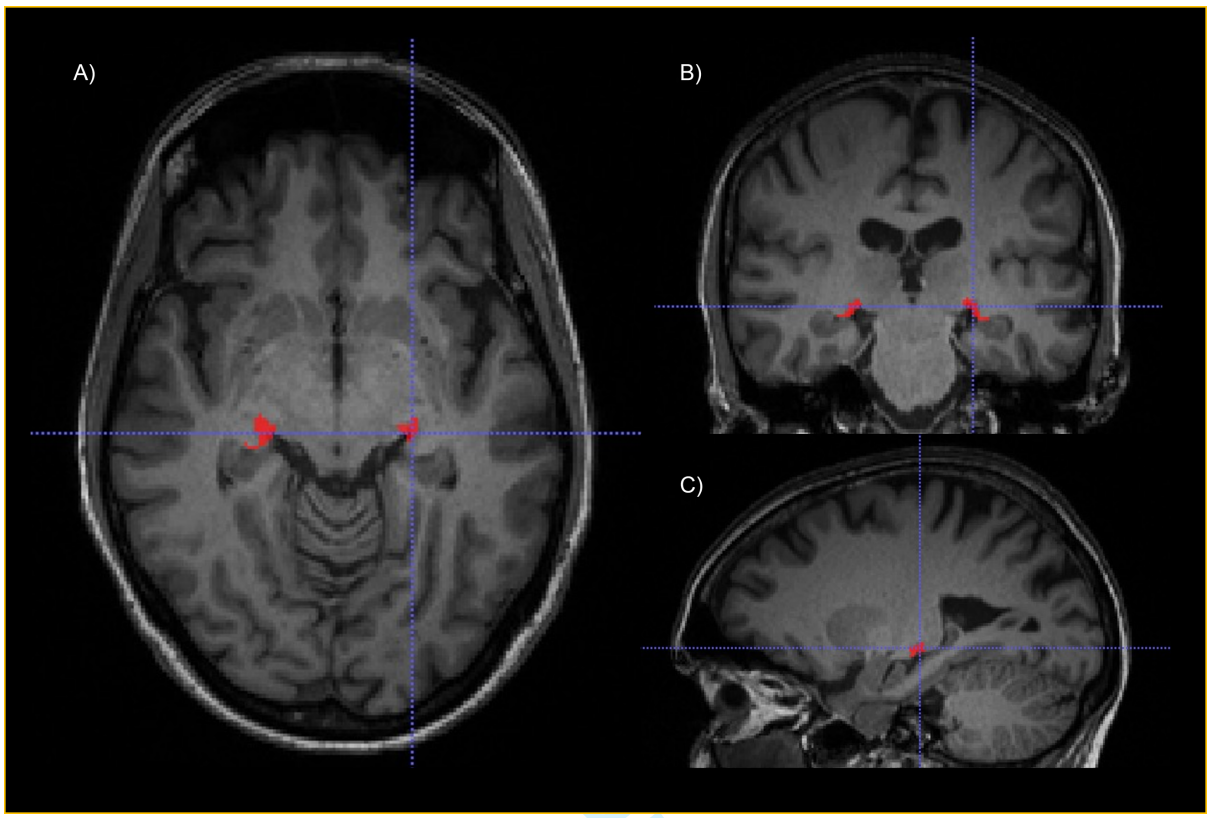

Legend: The figure shows an example of the lateral geniculate nucleus (LGN) segmentation in a control subject, as performed by the MAGeT brain algorithm[1,2]. The LGN is shown in red at: A) axial, B) coronal and C) sagittal view, on a 3D T1-weighted magnetization prepared rapid acquisition gradient echo (MPRAGE) sequence.

Supplementary Figure 2: VPN Segmentation by MAGeT

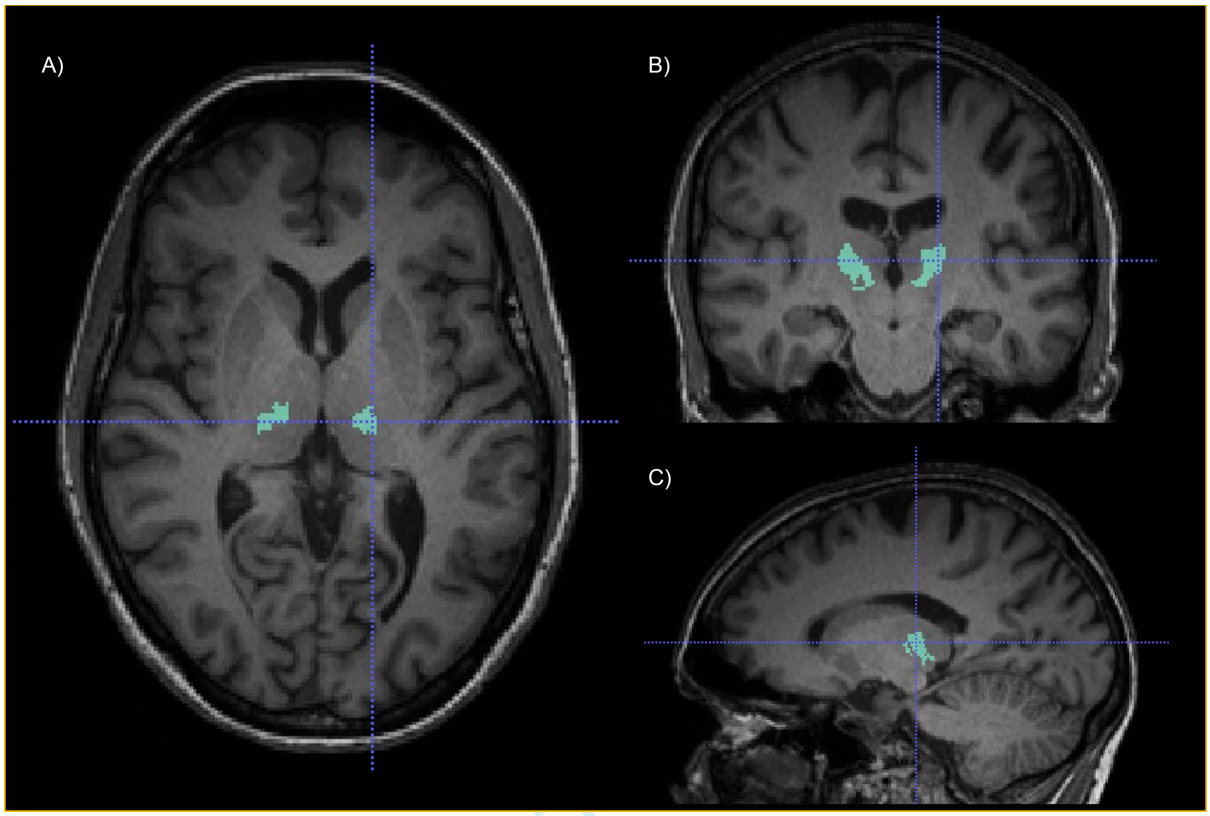

Legend: The figure shows an example of the ventral posterior nucleus (VPN) segmentation in a control subject, as performed by the MAGeT brain algorithm[1,2]. The VPN is shown in turquoise at: A) axial, B) coronal and C) sagittal view, on a 3D T1-weighted magnetization prepared rapid acquisition gradient echo (MPRAGE) sequence.

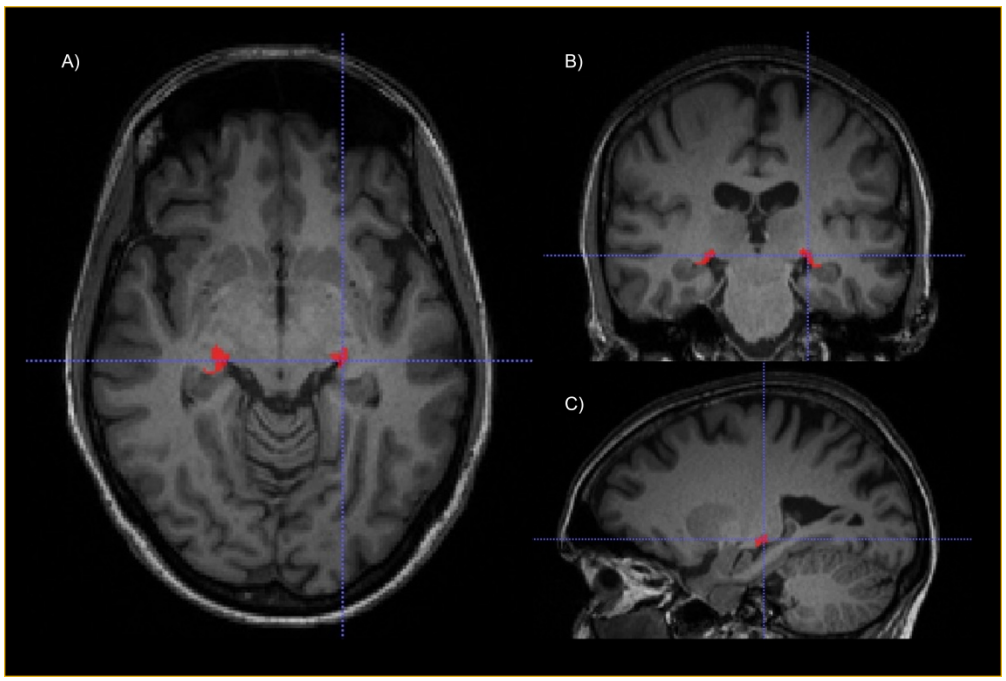

403x270mm (300 x 300 DPI)

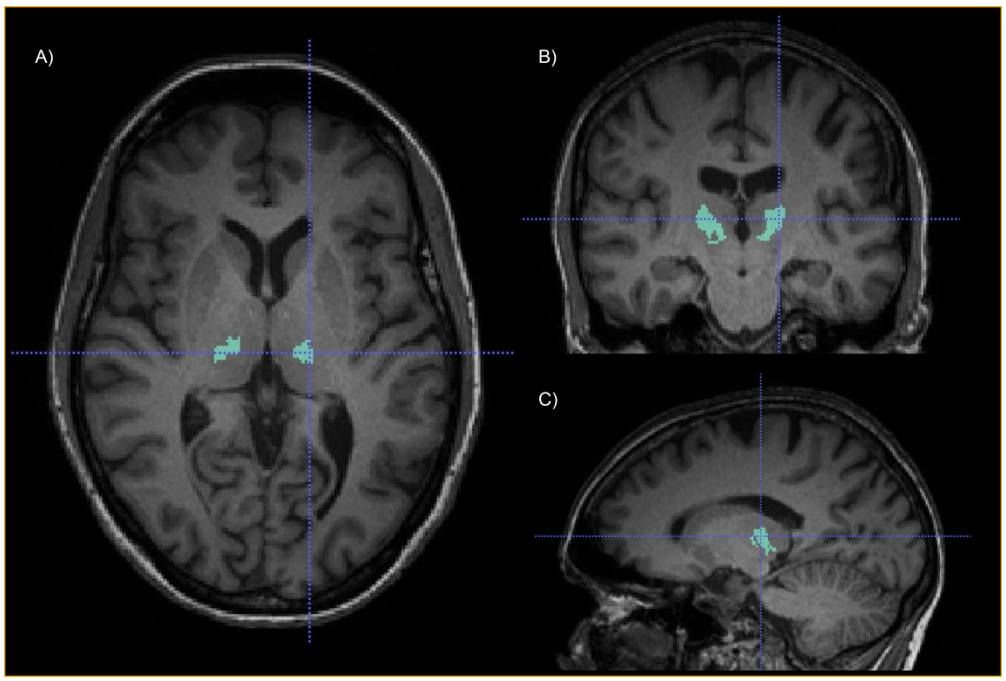

403x270mm (300 x 300 DPI)